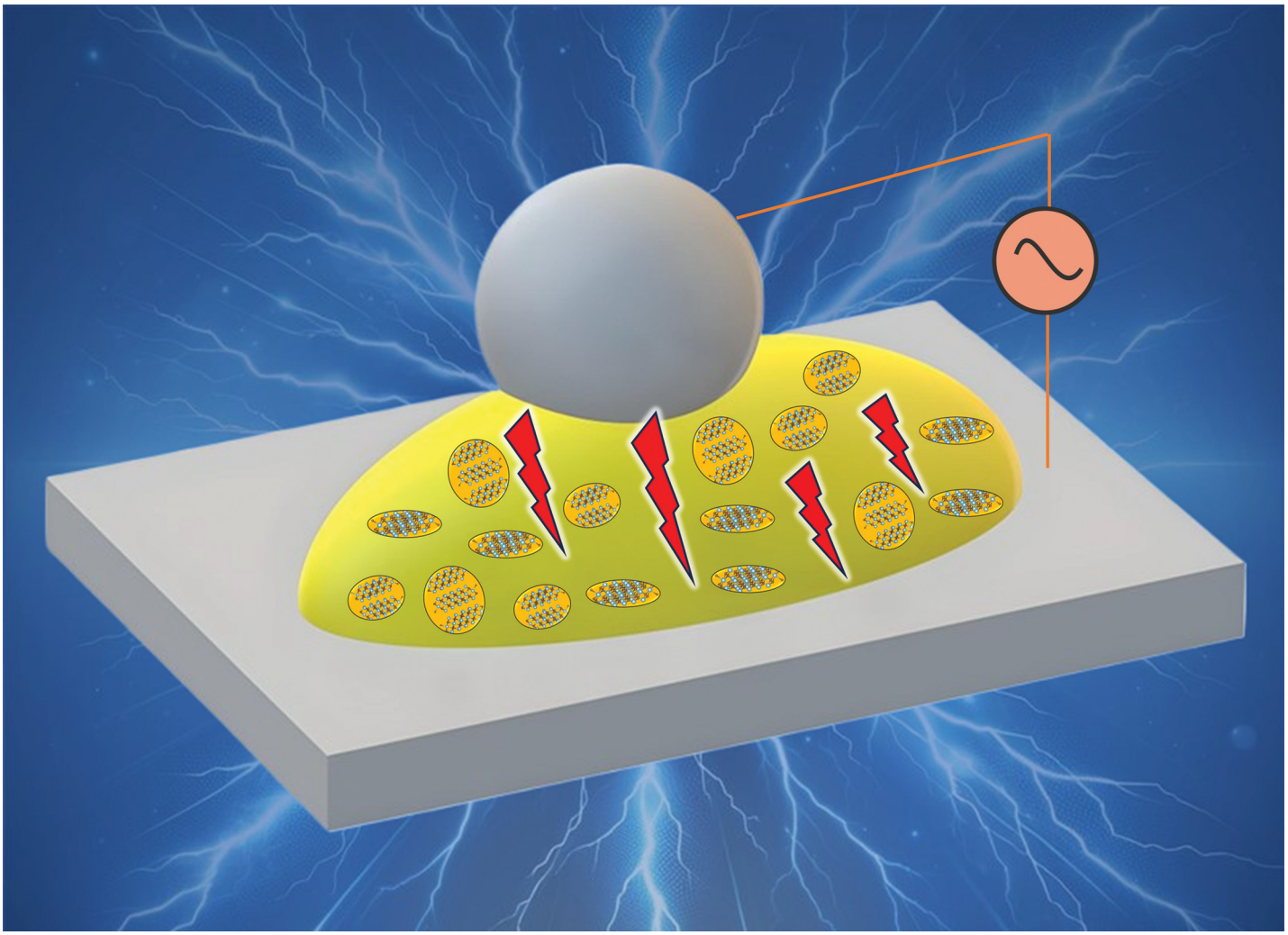

Showcasing research from Professor Hong Liang's Surface Science laboratory, Mechanical Engineering, Texas A&M University, College Station, Texas, USA

Tribo-electrical evaluation of conductive fluid film of $Ti_3C_2T_z$ MXene-containing lubricant

This research utilized an integrated approach to measure the impedance of a mineral oil consisting of (ML)-$Ti_3C_2T_z$ MXene nanoparticles as additive. It was revealed that the addition of 0.06 wt% of ML-$Ti_3C_2T_z$ MXene reduces friction for up to 60% compared to pure mineral oil. The additive in addition increased the lubricant's electrical conductivity and promoted rapid formation of a lubricating film between two steel surfaces.

The cover image was created by M. Humaun Kabir, a Ph.D. student at the Texas A&M University.

As featured in:

See Hong Liang *et al.*, *Mater. Adv.*, 2024, **5**, 5063.

ROYAL SOCIETY OF CHEMISTRY

rsc.li/materials-advances

Registered charity number: 207890

Materials Advances

ROYAL SOCIETY OF CHEMISTRY

PAPER

View Article Online
View Journal | View Issue

Cite this: *Mater. Adv.*, 2024, 5, 5063

Tribo-electrical evaluation of conductive fluid film of $Ti_3C_2T_z$ MXene-containing lubricant

Mohsen Tajedini,[a] Kailash Arole,[b] Zahra Ghasemi,[b] Rouzhina Azhdari,[a] Micah J. Green[bc] and Hong Liang*[ab]

Multi-Layer (ML)-$Ti_3C_2T_z$ MXene is being incorporated in lubricants to enhance their tribo-electrical performance. To date, a comprehensive understanding of the dynamic tribo-electrical behavior of lubricants containing nanomaterial enhancers is lacking. This study investigates a novel approach based on electrochemical impendence to analyze the tribo-electrical characteristics of light mineral oil with varying concentrations of (ML)-$Ti_3C_2T_z$ MXene as additive. We have modified a commercially available tribometer to integrate the impedance analyzer, allowing simultaneous evaluation of electrical performance during dynamic contact between two steel surfaces under sliding condition. This approach enables the measurement of friction, tracking impedance values, assessment of contact area, and the determination of oil film thickness. Our findings reveal that the addition of 0.06 wt% of ML-$Ti_3C_2T_z$ MXene reduces friction for up to 60% compared to pure mineral oil. Furthermore, the electrical conductivity can be increased by adding MXene in the mineral Oil. Lubricants have ML-$Ti_3C_2T_z$ MXene additives possess exceptional tribological and electrical characteristics, facilitating a rapid and conductive lubricating film formation to address current needs of lubrication in electrical vehicles (EVs). This enhances efficiency, extends component lifespan, and mitigates electrical-induced damages with reduced failure rates in EVs.

Received 22nd November 2023,
Accepted 22nd February 2024

DOI: 10.1039/d3ma01036h

rsc.li/materials-advances

Introduction

Advancement in the automotive industry demands the design of new lubricants to work at high speeds with less friction.[1] However, lubricating oils cannot attain the desired electrical resistance and friction values. The upcoming EV technology is still developing, and the demand to design suitable lubricants to avoid damage or wear is growing. One way to tackle this issue is the addition of nanomaterials in lubricants, which enhances tribological behavior and fluidic properties.[2–4] Graphene, MoS_2, and carbon nanotubes (CNTs) are generally added to the lubricants to alter their thermal and viscoelastic properties and ultimately enhance their tribological performance.[5–9] The high aspect ratio, excellent mechanical properties, good thermal conductivity, and lubricity make them an ideal lubricant additive candidate.

MXenes, a new member of two-dimensional (2D) material family, has shown promise in reducing friction and wear due to their layered structure of transition metal carbides.[10–13] So far, MXenes have caught considerable attention in the fields of energy storage,[14–18] polymer,[19] environments,[20,21] and thermal management.[22,23] Previous studies showed that adding limited amount of MXene to base oils such as polyalphaolefin (PAO) and silicon oil can reduce the coefficient of friction.[24] Moreover, this incorporation has demonstrated a potential to enhance thermal conductivity while decreasing the viscosity which is attributed to its non-Einstein behavior.[24,25] To exploit the superior features of MXene in tribological applications, the influence of these additives on the overall tribological behavior of lubricants exposed to electrical stimuli is yet to be understood. Bridging the gap between electrical properties and tribological performance is essential to solving current tribo-electrical challenges such as Electrically Induced Bearing Damages (EIBD).[26–28] The root cause of EIBD is current leakage from the stator passing the bearing towards the shaft. This, in turn, can create micro pitting and intense wear on the bearing resulting in bearing failure.[29] The current leakage can also affect the other tribopairs in drive units, such as gears, leading to surface damages. Evaluating ML-$Ti_3C_2T_z$ MXenes-induced conductive lubricating films in mineral oil through impedance analysis presents a promising avenue for comprehensively understanding their behavior under operational conditions.

The initial attempt utilizing electrochemical impendence to measure the fluid film thickness under shear at various

[a] *Mike Walker '66 Department of Mechanical Engineering, Texas A&M University, College Station, TX 77843-3123, USA. E-mail: hliang@tamu.edu*
[b] *Department of Materials Science & Engineering, Texas A&M University, College Station, TX 77843, USA*
[c] *Artie McFerrin Department of Chemical Engineering, Texas A&M University, College Station, TX 77843, USA*

temperatures was done by ourselves as reported by Chen *et al.*[30] In that work, we evaluated the relationship between impedance and fluid film thickness in the hydrodynamic regime of pure PAO base oil. The introduction of a solid additive can alter the contact mechanics between two surfaces resulting in alteration of electrical resistance mainly due to the possibility of occurring surface reactions under sliding.[30,31]

Continuing our previous approach be Chen *et al.*, we assessed the tribo-electrical behavior of a mineral oil. We evaluated the effects of MXene nanoparticles as additives on lubrication. We calculated the contact area in addition to the film thickness, and evaluated the tribo-performance in a broader regime, from boundary to hydrodynamic lubrication.

Electrochemical Model. The contact in this study is illustrated in Fig. 1. The Fig. 1a demonstrates two lubricated metallic contacts with the presence of asperities. The existence of asperities prevents complete contact between two surfaces. The real contact area is usually smaller than the nominal contact area (defined in the Hertzian contact mechanic). To provide a meaningful explanation of this, the actual contact area for a lubricated surface is visually represented on the underlying surface. Refer to the black-shaded oval in Fig. 1a for illustration. The tribofilm forms when the nano lubricants are sandwiched between asperities or there is a reaction between the lubricant and the surface (Fig. 1a).[32] The conventional understanding of electrical contact resistance proves inadequate in elucidating surface contact phenomena in lubricated contacts. This limitation arises due to the capacitive nature of the lubricant, diverging from a simple resistive behavior.[33]

By conceptualizing the contact region as an electrical circuit, we can determine the overall resistance of the circuit by combining the resistance of the bulk materials with the resistance within the contact area. The Hersey number, a critical parameter of tribo=condition, is calculated by dividing the product of velocity and viscosity by the applied load. This dimensionless quantity effectively captures the behavior of fluid flow within the system. Specifically, in the boundary and mixed lubrication regimes, associated with lower Hersey numbers, the contact's electrical behavior involves capacitances and resistances arranged in parallel, as illustrated in Fig. 1b. The contact resistance is composed of summation of the resistance of asperity contact ($R_{a.c}$) and solid tribofilm (R_t). As we approach to hydrodynamic regime, the influence of R_t becomes dominant in governing the total resistance. In this regime, due to the absence of any asperity contacts, the circuit is transformed into

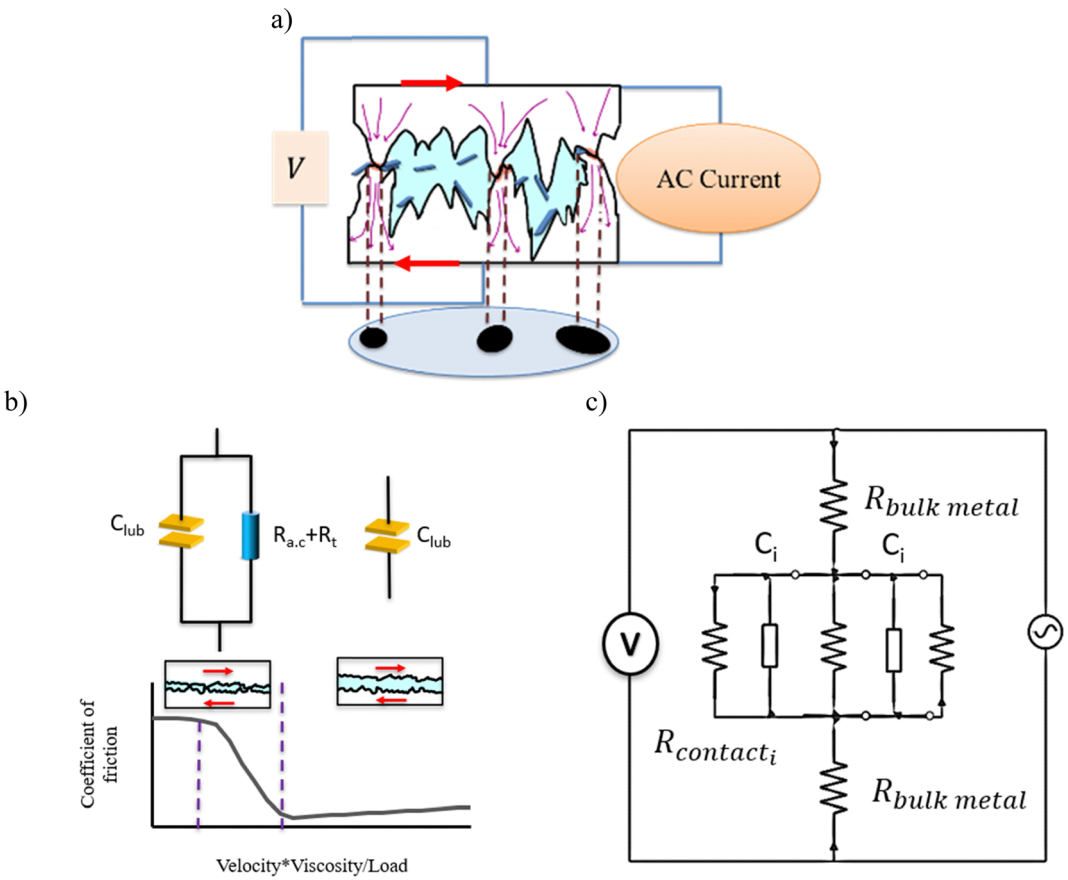

Fig. 1 (a) The lubricated contact mechanism, including asperities and nanoparticles. The red arrows show the movement direction, and the blue sheets demonstrate the ML-MXene particles, which can act as tribofilm, altering the contact resistance. Moreover, the purple arrows show the current path. The black projected areas are the real contact areas between asperities. (b) The electrical circuit models attributed to boundary and hydrodynamic regimes considering the stribeck curve and contact mechanism. (c) The proposed electrical circuit for a lubricated contact in the boundary lubrication regime.

a capacitor that represents the behavior of the lubricant.[34] The fluid film thickness in the hydrodynamic regime has a correlation with the imaginary part of the impedance.[35] In the boundary and mixed lubrication regimes, the presence of tribofilm and asperity contacts leads to a scenario similar to multiple capacitors and resistors arranged in parallel. Capacitance represents the fluid component (C_{lub}), while resistance is the combined effect of asperity contact resistance ($R_{a.c}$) and tribofilm resistance (R_t).

The proposed electrical circuit model is explaining the boundary and mixed lubrication regimes for the two metallic surfaces with asperities in contact (Fig. 1c). Each asperity in contact with the opposing surface has a resistance, which is in parallel with other resistances. The tribofilm forms when the nanolubricants are sandwiched between asperities (Fig. 1a) and the incorporated nanoparticles increase the resistance of asperities as if they are in series. Additionally, the effect of lubricant in the space between the asperity's contacts is considered as capacitors in parallel with the resistances.

Fig. 1c is the schematic of corresponding electric circuit of modified tribometer setup. By summing the resistances of the bulk materials and contact area and comparing it with the dynamically measured values, we can obtain information on the contact behaviour, including the effect of nanoparticle additives on the tribofilm, hence the total resistance of contact can be calculated as eqn (1).

$$R_{total} = R_{bulk\ metal} + R_{contact} \quad (1)$$

where, R_{total}, $R_{bulk\ metal}$, $R_{contact}$ are the resistance of total circuit, the tribopair, and the contact interfaces between asperities, respectively. The resistance of bulk metals can be calculated as follows:[36]

$$\frac{1}{R_{bulk\ metal}} = \sum \frac{\rho_i L_i}{A_0} \quad (2)$$

In this equation ρ_i, L_i, A_0 are the electric resistivity of metallic parts, the thickness along which the current flows, and the nominal contact area of each specimen, respectively. Sharvin's contact resistance equation estimates the real contact area (A) between the surfaces:[37]

$$A = \frac{\lambda(\rho_1 + \rho_2)}{2R_{contact}} \quad (3)$$

The variable λ represents the average distance an electron can travel between collisions, referred as the electron mean free path. Through combination of eqn (1)–(3), we can derive the real contact area (eqn (4)).

$$A = \frac{\lambda(\rho_1 + \rho_2)}{2\left(R_{total} - \sum \frac{\rho_i L_i}{A_0}\right)} \quad (4)$$

Continuous monitoring of the impedance while the surfaces are sliding leads to the estimation of the changing contact area of lubricated surfaces.

Using the impedance, we can better understand the effect of the addition of the ML-$Ti_3C_2T_z$ Mxenes to the base oil's electrical conductivity and film thickness. Because of their small dimensions, ML-$Ti_3C_2T_z$ Mxenes rapidly reduce the chance of asperity–asperity contacts. Additionally, the shear force needed to detach the layer is smaller than the plastic deformation of the asperities.

Results and discussion

The microstructure and configuration of MXene were characterized. The X-ray diffraction (XRD) patterns of dried ML-$Ti_3C_2T_z$ MXenes (Fig. 2a) powder were acquired using a Bruker D8 X-ray diffractometer with a LynxEye detector. The measurement was conducted in a Bragg–Brentano geometry, employing a CuKa (wavelength = 1.54 Å) radiation source. The X-ray scanning procedure involved using a step size of 0.02° and a scan rate of 1.5 seconds per step. Fig. 2a reveals the intensity of the (002) plane peak of MXene in the prepared samples. The (002) plane peak is a distinctive feature in the diffraction pattern corresponding to the MXene material's crystallographic planes.[11,38,39] A Veeco FPP 5000 Four Point Probe was used to measure the electrical conductivity

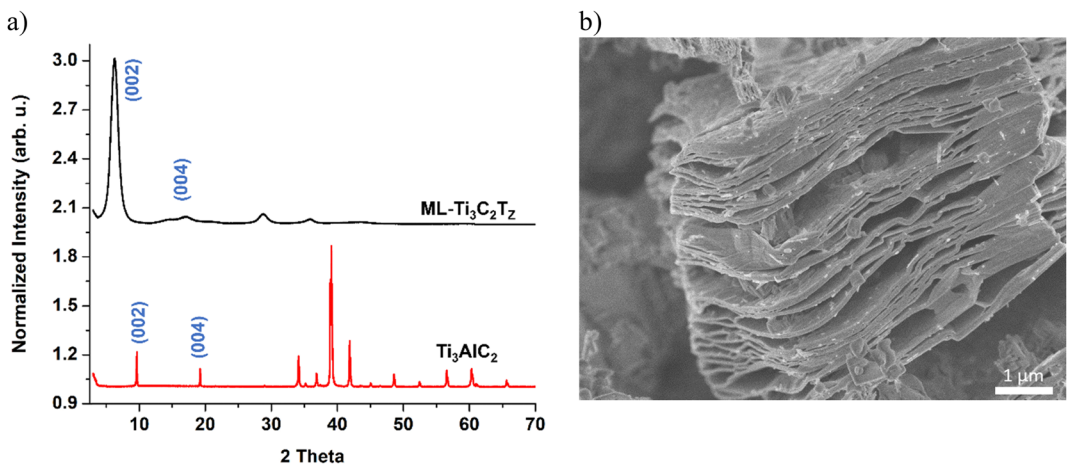

Fig. 2 (a) XRD of ML-$Ti_3C_2T_z$ MXene. (b) SEM of ML-$Ti_3C_2T_z$ MXenes.

of an ML-MXene filtered and bucky paper sample. The bucky paper was carefully prepared, dried, and used as the sample for the measurement. The recorded electrical conductivity value yielded a noteworthy 1208 s cm^{-1}.

In our experiment, different concentrations of ML-$Ti_3C_2T_z$ MXenes powder (0.01, 0.02, 0.04, and 0.06 wt%) were added into light mineral oil and then stirred using a magnetic stirrer and bath sonication. This procedure has been reported by us and others as in ref. 24 and 25. We observed the samples to see the transparency and any signs of aggregation. Those samples exhibited stability lasting a minimum of three days, indicating acceptable suspensibility in the same period. The inadequate colloidal stability of fluids may be attributed to the hydrophilic characteristics of ML-$Ti_3C_2T_z$.[40] Hence, higher concentrations result in particles settling sooner after dispersion, or even during the tribotest, potentially leading to agglomeration and an increase in the coefficient of friction. On the other hand, lower concentrations does not supply enough tribofilm to reduce the coefficient of friction.[25] Fig. 2b demonstrates the SEM image of the etched ML-$Ti_3C_2T_z$ MXenes which clearly shows the classical accordion like structure indicating the successful removal of Al and formation of MXene.[41] The large surface area and ability shear under sliding condition makes MXene a great choice for this work. Sheard MXene layer can alter the fluidic properties which will ultimately alters the film thickness under shearing.[42,43]

We have utilized an impedance analyzer and tribometer to evaluate the tribo-electrical performance of a lubricant containing ML-$Ti_3C_2T_z$ MXenes additives under dynamic (tribometer in operation) contact between steel surfaces. Initially, all steel substrate used in this work were polished on chemical mechanical polisher to ensure a uniform roughness of substrates. The ball material was E52 100, and the substrate was 4130 low-carbon steel. A load of 1*N* was applied, and a hertzian contact pressure of 0.63 MPa was consistently employed in all the tests. The linear speed was 5 cm s^{-1} to remain in the mixed lubrication regime. The temperature was kept at 80 °C, which falls within the operating temperature range of electric vehicles' drive units (0–100 °C).[44] The selection of this temperature mimics the actual operation of EVs and therefore data collected from this setup can be very useful to understand the failures of EVs. The tribo test results compare the effect of different ML-$Ti_3C_2T_z$ MXenes concentrations on the friction performance (Fig. 3). The addition of MXene into a base oil resulted in a decrease of friction with increased loading of MXene content. The layers of MXene are held together by relatively weak van der Waals forces. When subjected to shear forces, which arise from the frictional contact of tribopairs (surfaces sliding against each other), these weak forces can be overcome. This allows the layers to be separated or delaminated, resulting in the formation of single or a few layers of nanosheets.[45,46] This leads to metal/metal contact suppressing the coefficient of friction. Moreover, the addition of MXene into a base oil also produced a friction curve which is much more stable (less noise or fluctuation) than the pure base oil. The generated MXene nanosheets can fill up the produced wear tracks resulting in reduced friction and stable friction curves. Overall, the addition of 0.06 wt% of ML-$Ti_3C_2T_z$ MXene resulted in a drop in friction by 60% compared to mineral oil.

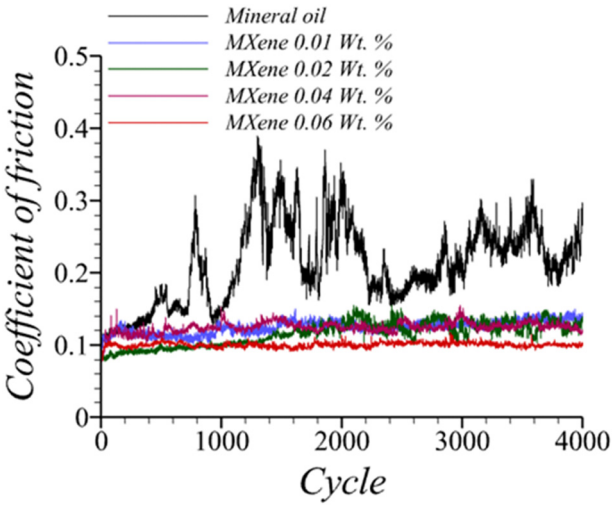

Fig. 3 The coefficient of friction results from different concentrations of MXene in the light mineral oil at 80 °C.

The impedance was recorded during the tribotests using a high frequency of 20 kHz. High frequency can increase accuracy. An alternating current (AC) voltage of 1 mV rms and a direct current DC-biased voltage of 0.5 mV were applied to ensure precise measurements and effectively address the high-impedance system. A small DC-biased voltage helps maintain the system's polarity for more consistent impedance measurements. The electrical resistance of different concentrations of ML-$Ti_3C_2T_z$ MXenes in mineral oil is demonstrated in Fig. 4. Each color represents a impedance values for specified ML-$Ti_3C_2T_z$ MXene concentration. To better exibit the results, the trends are shown with dashed lines. The first couple of cycles of tribo tests is called run-in, in which a slight initial wear produces a larger contact area between the ball and the plate.[47] As depicted in Fig. 4a, the real part of impedance (Re(Z)) at the run-in test is decreasing for all tests, which confirms the higher contact area due to asperity deformation and wear. This resistance drop was also reported in previous studies.[48] The decrease in resistance is notably sharper for the mineral oil, particularly highlighting its pronounced increase in the friction coefficient during the run-in period, as depicted in Fig. 3. However, upon the addition of ML-$Ti_3C_2T_z$ MXenes, there is a slight increase in friction and a minor decline in resistance.

After the run-in period, Re(Z) It starts increasing for the samples lubricated with oils containing additives, while the one lubricated with pure mineral oil remains almost constant. This can be attributed to the thicker ML-$Ti_3C_2T_z$ MXenes tribofilm formation, leading to more asperity/particle contact than asperity/asperity contact. Specifically, 0.06 wt% MXene shows the highest real part of the impedance and highest slope as compared to the mineral oil. Overall, a higher concentration of MXene increases the likelihood of asperity/particle contact, resulting in a more significant elevation of resistance so it is

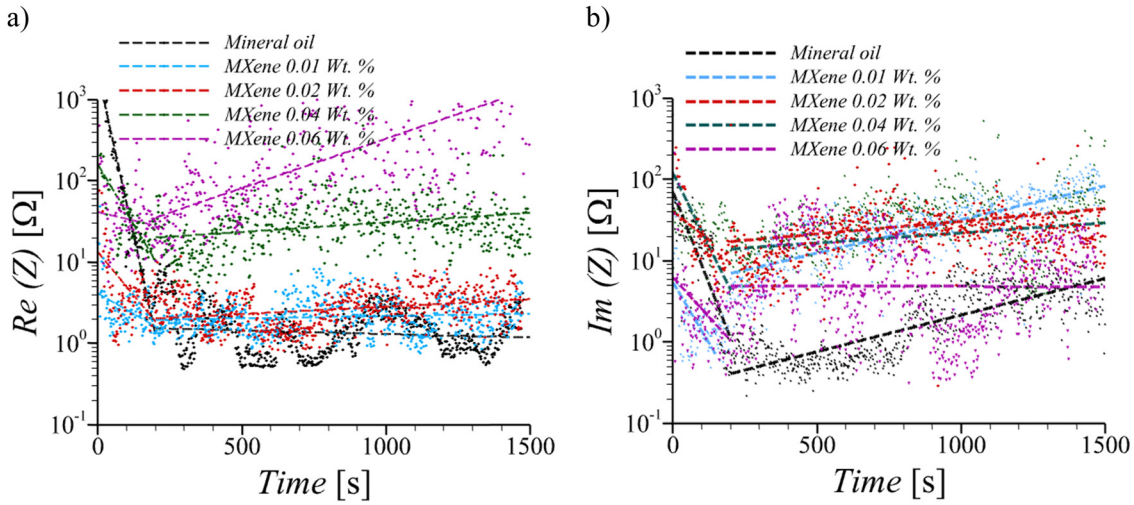

Fig. 4 The variation of the (a) real and (b) imaginary parts of the impedance *vs.* time in linear, logarithmic scale throughout the tribo tests of the lubricated surfaces with different concentrations of MXene in the light mineral oil at 80 °C.

very important to design the nanolubricants with an optimal concentration of MXene to obtain desired results.

By adding up to 0.02 wt% MXene, Re(Z) does not increase much, while Im(Z) dominates the Re(Z) (Fig. 4). This dominance indicates a significant contribution from reactive components originating from the fluid film, rapidly forming a sufficiently thick tribofilm that reduces friction. Therefore, the high Im(Z) (C_{lub}) and a low real part ($R_t + R_{a.c}$) indicate that MXene exhibits reactive behavior with minimal electrical resistance (Fig. 4). In other words, the portion of the R_t is higher than $R_{a.c}$.

During the run-in (initial runs of the test), Im(Z) decreases and then starts to increase for all samples (Fig. 4b). Pure mineral oil shows the lowest impedance, demonstrating thinner oil film thickness (C_{lub}) compared to the MXene-added lubricants. Lower impedance represents a lower oil thickness trapped between the asperities.[30,35]

Conclusions

To conclude, the addition of MXene to the mineral oil results in an increase in impedance while reducing friction. The increase in resistance is attributed to metal/particle contact resistance, which can reduce the possible electrical damage due to the potential difference between the tribopairs.[49] The addition of low concentrations of MXene results in a limited increase in (Re(Z)), while the (Im(Z)) increases. These changes indicate the significant friction reduction due to sufficiently high fluid film thickness, ultimately facilitating effective friction reduction. When high Re(Z) and low Im(Z) are required, 0.06 wt.% could be a good candidate.

On the other hand, when the opposite effect is required, 0.02 wt% of MXene can be more suitable. This indicates that the concentration of MXene in oil plays a vital role and can help design the nano lubricants for the desired applications. More importantly, MXene causes the rapid formation of a film consisting of an oil, leading to friction reduction. The mechanisms of this phenomenon are currently being investigated. Our results provide valuable insights into the tribological and electrical properties of lubricants containing $Ti_3C_2T_z$ MXene additives and have practical implications for developing high-performance lubricants.

Conflicts of interest

There are no conflicts to declare.

Acknowledgements

The authors would like to thank the TAMU Materials Characterization Facility, Microscopy & Imaging Center for their support to this work.

References

1 L. I. Farfan-Cabrera, Tribology of electric vehicles: A review of critical components, current state and future improvement trends, *Tribol. Int.*, 2019, **138**, 473–486.
2 L. Duan, J. Li and H. Duan, Nanomaterials for lubricating oil application: A review, *Friction*, 2023, **11**(5), 647–684.
3 X. He, H. Xiao, H. Choi, A. Díaz, B. Mosby, A. Clearfield and H. Liang, α-Zirconium phosphate nanoplatelets as lubricant additives, *Colloids Surf., A*, 2014, **452**, 32–38.
4 L. Fang, S. Korres, W. A. Lamberti, M. N. Webster and R. W. Carpick, What stress components drive mechanochemistry? A study of ZDDP tribofilm formation, *Faraday Discuss.*, 2023, **241**, 394–412.
5 W. Dai, B. Kheireddin, H. Gao and H. Liang, Roles of nanoparticles in oil lubrication, *Tribol. Int.*, 2016, **102**, 88–98.
6 S. Saha, P. Lakhe, M. J. Mason, B. J. Coleman, K. Arole, X. Zhao, S. Yakovlev, S. Uppili, M. J. Green and R. A. Hule, Sustainable production of graphene from petroleum coke

using electrochemical exfoliation, *npj 2D Mater. Appl.*, 2021, **5**(1), 1–8.

7 C. Kumara, M. J. Lance and J. Qu, Macroscale superlubricity by a sacrificial carbon nanotube coating. Materials Today, *NANO*, 2023, **21**, 100297.

8 A. Seynstahl, M. Köbrich, T. Rosnitschek, M. Göken and S. Tremmel, Enhancing the lifetime and vacuum tribological performance of PVD-MoS2 coatings by nitrogen modification, *Surf. Coat. Technol.*, 2024, **477**, 130343.

9 K. Arole, Y. Chen, A. Delgado, J. Hubbard and H. Liang, Urea-ZrP nanoparticle-enabled electro-responsivity, *J. Mol. Liq.*, 2022, **363**, 119803.

10 J. Gao, C.-F. Du, T. Zhang, X. Zhang, Q. Ye, S. Liu and W. Liu, Dialkyl Dithiophosphate-Functionalized Ti3C2T x MXene Nanosheets as Effective Lubricant Additives for Antiwear and Friction Reduction, *ACS Appl. Nano Mater.*, 2021, **4**(10), 11080–11087.

11 S. Athavale, S. Micci-Barreca, K. Arole, V. Kotasthane, J. Blivin, H. Cao, J. L. Lutkenhaus, M. Radovic and M. J. Green, Advances in the Chemical Stabilization of MXenes, *Langmuir*, 2023, **39**(3), 918–928.

12 M. Naguib, V. N. Mochalin, M. W. Barsoum and Y. Gogotsi, 25th anniversary article: MXenes: a new family of two-dimensional materials, *Adv. Mater.*, 2014, **26**(7), 992–1005.

13 M. Chhattal, A. Rosenkranz, S. Zaki, K. Ren, A. Ghaffar, Z. Gong and P. G. Grützmacher, Unveiling the tribological potential of MXenes-current understanding and future perspectives, *Adv. Colloid Interface Sci.*, 2023, 103021.

14 S. Feng, X. Wang, M. Wang, C. Bai, S. Cao and D. Kong, Crumpled MXene electrodes for ultrastretchable and high-area-capacitance supercapacitors, *Nano Lett.*, 2021, **21**(18), 7561–7568.

15 J. Nan, X. Guo, J. Xiao, X. Li, W. Chen, W. Wu, H. Liu, Y. Wang, M. Wu and G. Wang, Nanoengineering of 2D Mxene-based materials for energy storage applications, *Small*, 2021, **17**(9), 1902085.

16 K. Arole, J. W. Blivin, A. M. Bruce, S. Athavale, I. J. Echols, H. Cao, Z. Tan, M. Radovic, J. L. Lutkenhaus and M. J. Green, Exfoliation, delamination, and oxidation stability of molten salt etched Nb 2 CT z MXene nanosheets, *Chem. Commun.*, 2022, **58**(73), 10202–10205.

17 J. Yan, L. Yu, D. Wang, W. Zhang, Z. Xiong, T. Nie, Z. Ji and X. Yan, MnO 2/MXene–Ti 3 C 2 T x flexible foam for use in lithium ion storage, *Mater. Adv.*, 2021, **2**(14), 4772–4780.

18 S. Saha, K. Arole, M. Radovic, J. L. Lutkenhaus and M. J. Green, One-step hydrothermal synthesis of porous Ti3C2Tz MXene/rGO gels for supercapacitor applications, *Nanoscale*, 2021, **13**(39), 16543–16553.

19 I. Amin, H. v d Brekel, K. Nemani, E. Batyrev, A. de Vooys, H. van der Weijde, B. Anasori and N. R. Shiju, Ti3C2T x MXene Polymer Composites for Anticorrosion: An Overview and Perspective, *ACS Appl. Mater. Interfaces*, 2022, **14**(38), 43749–43758.

20 G. Zou, J. Guo, Q. Peng, A. Zhou, Q. Zhang and B. Liu, Synthesis of urchin-like rutile titania carbon nanocomposites by iron-facilitated phase transformation of MXene for environmental remediation, *J. Mater. Chem. A*, 2016, **4**(2), 489–499.

21 H. Wang, N. Liu, L. Qu and B. Xu, Siloxane-decorated MXene nanosheet-reinforced EP composites with outstanding flame retardancy and liquid-oxygen compatibility for ultra-low-temperature applications, *New J. Chem.*, 2023, **47**, 13353–13366.

22 X. Chen, Biomimetic phase change materials for extreme thermal management, *Matter*, 2022, **5**(8), 2495–2497.

23 K. Arole, J. W. Blivin, S. Saha, D. E. Holta, X. Zhao, A. Sarmah, H. Cao, M. Radovic, J. L. Lutkenhaus and M. J. Green, Water-dispersible Ti3C2Tz MXene nanosheets by molten salt etching, *Iscience*, 2021, **24**(12), 103403.

24 K. Arole, M. Tajedini, A. Sarmah, S. Athavale, M. J. Green and H. Liang, Effects of Ti3C2Tz MXene nanoparticle additive on fluidic properties and tribological performance, *J. Mol. Liq.*, 2023, 122435.

25 A. Rosenkranz, M. C. Righi, A. V. Sumant, B. Anasori and V. N. Mochalin, Perspectives of 2D MXene Tribology, *Adv. Mater.*, 2023, **35**(5), 2207757.

26 A. García Tuero, N. Rivera, E. Rodríguez, A. Fernández-González, J. L. Viesca and A. Hernández Battez, Influence of additives concentration on the electrical properties and the tribological behaviour of three automatic transmission fluids, *Lubricants*, 2022, **10**(11), 276.

27 G. Boidi, J. C. F. de Queiróz, F. J. Profito and A. Rosenkranz, Ti3C2T x MXene Nanosheets as Lubricant Additives to Lower Friction under High Loads, Sliding Ratios, and Elevated Temperatures, *ACS Appl. Nano Mater.*, 2022, **6**(1), 729–737.

28 W. Dai, Y. Chen, K. Lee, A. M. Sinyukov, M. Alkahtani, P. R. Hemmer and H. Liang, In situ investigation of the growth of a tribofilm consisting of NaYF4 fluorescent nanoparticles, *Tribol. Trans.*, 2018, **61**(3), 503–512.

29 S. Bond, R. L. Jackson and G. Mills, In *Electrified Mechanical Contact Arcing Surface Damage and Reduction by Silver Nanoparticle Enhanced Greases, 2023 IEEE 68th Holm Conference on Electrical Contacts (HOLM), IEEE*, 2023, pp 1–8.

30 Y. Chen and H. Liang, Tribological evaluation of electrical resistance of lubricated contacts, *J. Tribol.*, 2020, **142**(11), 114502.

31 J. Chen and W. Zhao, Simple method for preparing nanometer thick Ti3C2TX sheets towards highly efficient lubrication and wear resistance, *Tribol. Int.*, 2021, **153**, 106598.

32 W. Dai, K. Lee, A. M. Sinyukov and H. Liang, Effects of vanadium oxide nanoparticles on friction and wear reduction, *J. Tribol.*, 2017, **139**(6), 061607.

33 L. Wang, D. Snihirova, M. Deng, B. Vaghefinazari, D. Höche, S. V. Lamaka and M. L. Zheludkevich, Revealing physical interpretation of time constants in electrochemical impedance spectra of Mg via Tribo-EIS measurements, *Electrochim. Acta*, 2022, **404**, 139582.

34 J. Archard, Elastic Deformation and the Laws of Friction, *Proc. Roy. Soc. Scr. A*, 1957, **243**(1233), 190–205.

35 Y. Chen, P. A. Renner and H. Liang, Using electrochemical impendence to characterize thermal performance of

working lubricants, *Surf. Topogr.: Metrol. Prop.*, 2021, **9**(3), 035035.

36 H. Berger, Contact resistance and contact resistivity, *J. Electrochem. Soc.*, 1972, **119**(4), 507.

37 L. Kogut and K. Komvopoulos, Electrical contact resistance theory for conductive rough surfaces, *J. Appl. Phys.*, 2003, **94**(5), 3153–3162.

38 G. B. Tezel, K. Arole, D. E. Holta, M. Radovic and M. J. Green, Interparticle interactions and rheological signatures of Ti3C2Tz MXene dispersions, *J. Colloid Interface Sci.*, 2022, **605**, 120–128.

39 M. Nawaz, W. Miran, J. Jang and D. S. Lee, One-step hydrothermal synthesis of porous 3D reduced graphene oxide/TiO2 aerogel for carbamazepine photodegradation in aqueous solution, *Appl. Catal., B*, 2017, **203**, 85–95.

40 M. Ghidiu, M. R. Lukatskaya, M.-Q. Zhao, Y. Gogotsi and M. W. Barsoum, Conductive two-dimensional titanium carbide 'clay'with high volumetric capacitance, *Nature*, 2014, **516**(7529), 78–81.

41 S. Saha, K. Arole, M. Radovic, J. Lutkenhaus and M. Green, One-step hydrothermal synthesis of porous Ti3C2Tz MXene/rGO gels for supercapacitor applications, *Nanoscale*, 2021, **13**(39), 16543–16553.

42 D. F. Zambrano-Mera, M. I. Broens, R. Villarroel, R. Espinoza-Gonzalez, J. Y. Aguilar-Hurtado, B. Wang, S. Suarez, F. Mücklich, P. Valenzuela and W. Gacitúa, Solid lubrication performance of sandwich Ti3C2Tx-MoS2 composite coatings, *Appl. Surf. Sci.*, 2023, **640**, 158295.

43 P. Das, S. Ganguly, A. Rosenkranz, B. Wang, J. Yu, S. Srinivasan and A. R. Rajabzadeh, MXene/0D nanocomposite architectures: Design, properties and emerging applications, *Mater. Today Nano*, 2023, **24**, 100428.

44 R. Uerlich, S. Köller, G. Witham, T. Koch and L. Eckstein, Experimental validation of an automated approach for estimating the efficiency and heat balance of gearboxes based on an electrified heavy commercial vehicle axle, *World Electr. Veh. J.*, 2022, **13**(8), 142.

45 B. C. Wyatt, A. Rosenkranz and B. Anasori, 2D MXenes: tunable mechanical and tribological properties, *Adv. Mater.*, 2021, **33**(17), 2007973.

46 M. Naguib, T. Saito, S. Lai, M. S. Rager, T. Aytug, M. P. Paranthaman, M.-Q. Zhao and Y. Gogotsi, Ti 3 C 2 T x (MXene)–polyacrylamide nanocomposite films, *RSC Adv.*, 2016, **6**(76), 72069–72073.

47 Y. Xu, Q. Zheng, J. Geng, Y. Dong, M. Tian, L. Yao and K. D. Dearn, Synergistic effects of electroless piston ring coatings and nano-additives in oil on the friction and wear of a piston ring/cylinder liner pair, *Wear*, 2019, **422**, 201–211.

48 M. Fellah, N. Hezil, M. A. Hussein, M. A. Samad, M. Z. Touhami, A. Montagne, A. Iost, A. Obrosov and S. Weiss, Preliminary investigation on the bio-tribocorrosion behavior of porous nanostructured β-type titanium based biomedical alloys, *Mater. Lett.*, 2019, **257**, 126755.

49 S. Mischler, Triboelectrochemical techniques and interpretation methods in tribocorrosion: A comparative evaluation, *Tribol. Int.*, 2008, **41**(7), 573–583.